Materials Transactions, Vol. 52, No. 5 (2011) pp. 906 to 913
Special Issue on Aluminium Alloys 2010

Effects of Cu Addition on Behavior of Nanoclusters during Multi-Step Aging in Al-Mg-Si Alloys*[1]

JaeHwang Kim*[2], Equo Kobayashi and Tatsuo Sato

Department of Metallurgy and Ceramics Science, Tokyo Institute of Technology, Tokyo 152-8552, Japan

Two types of nanoclusters, i.e. Cluster (1) and Cluster (2), play a strongly important role in the bake-hardening (BH) response in Al-Mg-Si alloys. Different formation behaviors of two types of nanoclusters were studied by means of hardness, differential scanning calorimetry (DSC), electrical resistivity measurement, transmission electron microscopy (TEM) and high resolution TEM observation in the both Cu-free and Cu-added Al-Mg-Si alloys. As the results, Cluster (1) formed during natural aging at room temperature causes a deleterious effect, whereas Cluster (2) formed by the pre-aging at 100°C is effective for the suppression of the negative effect on the two-step aging behavior of the both Cu-free and Cu-added alloys. On the other hand, the microalloying of Cu strongly affects the nanocluster formation due to the strong interaction with Mg, Si atoms and vacancies. The first-principle calculation for the two-body interaction energies provides quite useful information to understand the early stage of the phase decomposition. The effects of nanoclusters and the Cu addition on the age-hardening behaviors of Al-Mg-Si alloys are discussed based on the multi-step age-hardening phenomena. [doi:10.2320/matertrans.L-MZ201121]

(Received October 1, 2010; Accepted January 18, 2011; Published April 13, 2011)

Keywords: *aluminum-magnesium-silicon alloy, age hardening, nanocluster, copper addition, multi-step aging*

1. Introduction

Age-hardenable Al-Mg-Si alloys have been widely used for body panels of automobiles due to their good precipitation hardening response during a paint bake treatment at 170°C for 1.2 ks, i.e., bake-hardening (BH). The precipitation sequence generally accepted in Al-Mg-Si alloys is

$$\text{SSSS} \rightarrow \text{GP zone} \rightarrow \beta'' \rightarrow \beta' \rightarrow \beta \qquad (1)$$

where SSSS is the super saturated solid solution.[1,2] However, as detected by the advanced instruments such as the three-dimensional atom probe (3DAP), the introduction of nano-scale clusters which considerably affects the formation of metastable phases is unavoidable in order to clarify the age-hardening phenomena. Recently, Serizawa *et al.*[3,4] introduced characteristics of two types of nanoclusters, i.e., Cluster (1) and Cluster (2), in the Al-Mg-Si alloys. By the introduction of two types of nanoclusters which play a strongly important role in the age-hardenable Al-Mg-Si alloys, the control of nanoclusters by the microalloying elements as well as the heat-treatment histories becomes very important in terms of that microstructure and mechanical properties strongly depend on the nanocluster formation at the early stage of the phase decomposition. Furthermore, "Nanocluster Assist Processing (NCAP)" proposed by Sato *et al.*[5] stimulates research for the nanocluster formation. Hoshino and Nakamura[6] and Hirosawa *et al.*[7–9] have proposed and calculated the interaction energy among solute atoms and vacancies in the Al-based alloys. On the other hand, there are several reports regarding the effects of the Cu addition on the age-hardening behavior of Al-Mg-Si alloys. Kim and Sato[10] confirmed two types of nanoclusters in the both Cu-free and Cu-added alloys. Furthermore, some effects such as enhancement of hardness, refinement of precipitates, precipitation sequence and interaction parameters among Cu atoms and solute atoms are investigated in Al-Mg-Si alloys.[5,11–14]

However, there are still controversial debates because of the poor understanding of nanoclusters in the both Cu-free and Cu-added Al-Mg-Si alloys. The goal of this study is, therefore, to investigate the role of the Cu addition and pre-aging treatment on the age-hardening phenomena in Al-Mg-Si alloys. The age-hardening behaviors are discussed based on the multi-step aging phenomena in this study. Meanwhile, heat-treatments in this study are designed in order to understand the role of two types of nanoclusters as well as the Cu addition on the age-hardening behaviors.

2. Experimental Procedure

The Cu-free Al-Mg-Si alloy, AA6022, and Cu-added Al-Mg-Si alloy, AA6111, are used in this study. The chemical compositions are described in Table 1. The specimens were solution-treated at 560°C for 1.8 ks, subsequently quenched into ice-water and held for 60 s. In the present study, three ways of the heat-treatment are designed after ice-water quenching in order to understand the effect of the nanocluster formation on the age-hardening behaviors. Firstly, isothermal aging at 100 and 170°C after quenching was directly performed. Secondly, the natural aging (N.A.) for 604.8 ks followed by isothermal aging at 170°C was performed. Lastly, the pre-aging (P.A.) at 100°C for 3.6 ks followed by the natural aging for 604.8 ks and isothermal aging at 170°C for up to 2419 ks (approximately 1 month) were also performed. Differential scanning calorimetry (DSC), a useful technique for detection of nanoclusters, was operated using a Rigaku equiptment of DSC823D/TAS-200 ranging from −50°C to 500°C with 30 mg Al(99.99%) as a reference under an argon atmosphere with different heating rates of 2 and 10°C/min. Micro Vickers hardness measurements were employed using Mitsutoyo HM-102. Averaged five data out of seven data were used where specimens were prepared

*[1]The Paper Contains Partial Overlap with the ICAA12 Proceedings by USB under the Permission of the Editorial Committee.
*[2]Graduate Student, Tokyo Institute of Technology

Table 1 Chemical compositions of the used alloys [mass%].

Alloy	Mg	Si	Cu	Mn	Fe	Ti	Zn	Cr	Al
AA6022	0.612	0.979	0.001	0.119	0.117	0.006	0.004	0.044	Bal.
AA6111	0.621	0.994	0.727	0.120	0.129	0.055	0.005	0.044	Bal.

wihin 0.3 ks just after each heat-treatment in order to minimize the natural aging effect. Electrical resistivity measurements were preformed by a four-probe method. Transmission electron microscopy (TEM) was carried out to observe nanoclusters and nano-precipitates using JEM3010 with 300 kV.

3. Analysis Method of Electrical Resistivity

All specimens for the electrical resistivity measurement were prepared as wires with the diameter of 1.0 mm and the gage length of 300 mm. Electrical resistivity was measured at −196°C using liquid nitrogen by a four-probe method with 120 mA direct current. By this method, the thermal scattering effect on the resistivity can be neglected due to the low temperature measurements.[15] Electrical resistivity is calculated using the following equation.

$$\rho = V_m/I_{st} \times A/L[\Omega m] \quad (2)$$

where, ρ, I_{st}, A, V_m and L represent resistivity, constant current (120 mA), area of a cross section of a specimen (7.854×10^{-7} m^2), electric potential difference (experimental measurement, mV) and the gage length (300 mm).

The electrical resistivity is increased by the interrupting crystal periodicity. The electrical resistivity in an alloy is mainly caused by the thermal vibration of atoms, solute atoms and precipitates. Osamura *et al.*[15] investigated the changes of the electrical resistivity in the Al-Zn alloys through the two-band model. With their proposal, the electrical resistivity can be expressed as below.

$$\rho = \rho_0 + \rho_m + \rho_p \quad (3)$$

where ρ_0, ρ_m and ρ_p represent resistivity by the lattice vibration in the pure Al, solute atoms in the matrix and precipitates, respectively. Meanwhile, ρ_0 is not changed during isothermal aging for the electrical resistivity measurement and ρ_m does not depend on the temperature, but concentration of the solute atoms. Among them, ρ_p strongly affects the changes of electrical resistivity through the formation of precipitates with different size, number density and size distribution. Besides, ρ_p can be expressed as below.

$$\rho_p = N_p \times G_p(r) \quad (4)$$

where, N_p and $G_p(r)$ represent the number density of precipitates per unit volume and resistivity from one precipitate with radius r. Furthermore, V_p, volume of the precipitate, is represented as below.

$$V_p = N \times 4\pi r^3/3 \quad (5)$$

Namely, the number density of precipitates is substantially decreased with increase of the radius of a precipitate. From this basis, the maximum of the electrical resistivity is drawn during isothermal aging. The electrical resistivity change during isothermal aging is simply expressed using a dotted line in Fig. 1 regarding the size and number density changes with aging time.

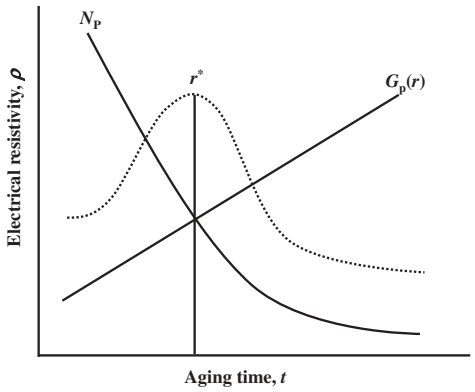

Fig. 1 Schematic diagram of the electrical resistivity change regarding the radius and number density change of precipitates during isothermal aging.

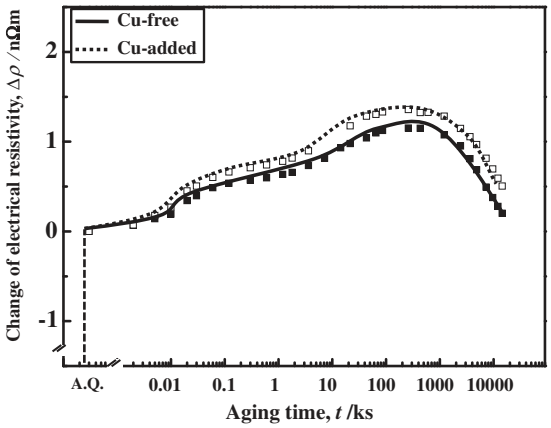

Fig. 2 Changes of the electrical resistivity during aging at 100°C in the both Cu-free and Cu-added alloys.

4. Results

Figure 2 shows the changes of electrical resistivity during aging at 100°C in the both Cu-free and Cu-added alloys. It is confimed that the Cu-added alloy shows higher number density of Cluster (2) than the Cu-free alloy. Figure 3 shows the hardness results during aging at 100°C in the both Cu-free and Cu-added alloys. As confrimed by the electrical resistivity, the Cu-added alloy represents the higher hardness than the Cu-free alloy. The reason why Cu enhances the formation of Cluster (2) is discussed in the next section. Figure 4 shows the DSC results with different heat-treatment conditions in the both Cu-free and Cu-added alloys. The limited temperatures ranging from 150 to 350°C is shown in order to clearly express the peaks of the nanoclusters and strengthening phase. There are exothermal peaks at 249 and 240°C for the as-quenched Cu-free and Cu-added alloys, respectively. Miao and Laughlin[14,16] previously revealed that the peak at around 250°C is due to the formation of the β'' phase in the both Cu-free and Cu-added alloys. In the case of the N.A. specimens for 604.8 ks, the peak emerges at 253 and 250°C for the Cu-free and Cu-added alloys, respectively. The

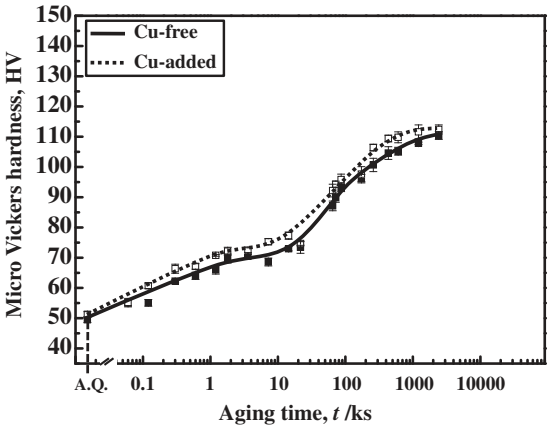

Fig. 3 Changes of the hardness during aging at 100°C in the both Cu-free and Cu-added alloys.

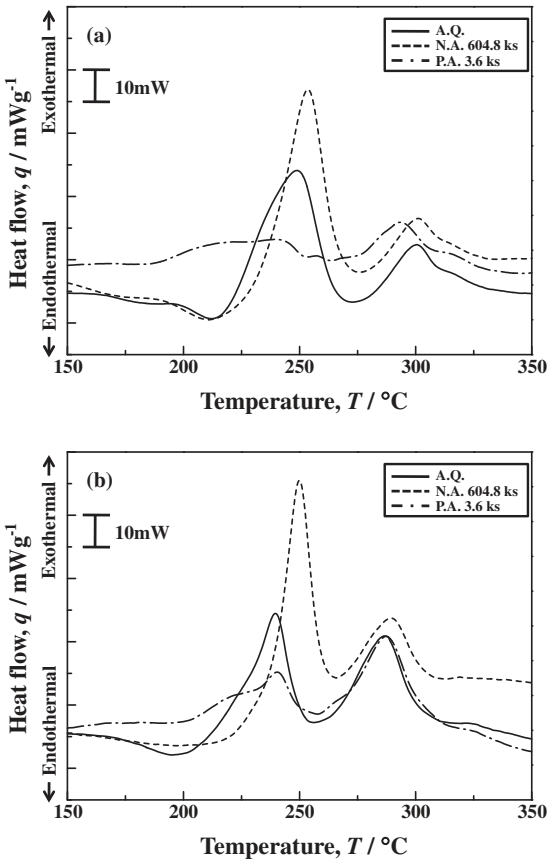

Fig. 4 DSC results with different heat-treatment conditions in the both (a) Cu-free and (b) Cu-added alloys.

peak temperature of the β'' phase is shifted to the higher temperature with the N.A. treatment in the both Cu-free and Cu-added alloys. It is deduced that Cluster (1) formed during natural aging retards the transformation into the β'' phase. On the other hand, one more exothermic peak, as a shoulder at 216°C, appeared in the P.A. specimens in the both Cu-free and Cu-added alloys. The peak of the β'' phase also appeared at 239 and 240°C in the both Cu-free and Cu-added alloys, respectively. It is also deduced that the formation of Cluster (2) by P.A. makes it easier to transform into the β'' phase since the appearance of the shoulder at 216°C and lower area

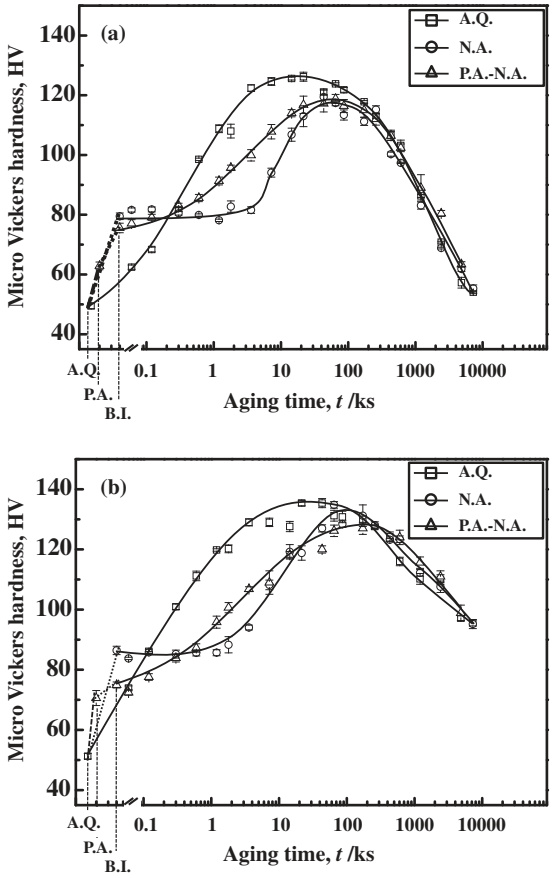

Fig. 5 Hardness changes during isothermal aging at 170°C with different heat-treatment conditions in the both (a) Cu-free and (b) Cu-added alloys. A.Q.: as-quenched, P.A.: as-pre-aged, B.I.: before isothermal aging

of the peak of the β'' phase than the other heat-treatment histories represents lower energy requirement for the formation of the β'' phase in the both Cu-free and Cu-added alloys.

Figure 5 shows the hardness measurement results during isothermal aging at 170°C as a function of aging time in the both Cu-free and Cu-added alloys. The results of the A.Q. and B.I. (before isothermal aging) with conditions of N.A. and P.A.-N.A. are represented in Fig. 5 to know the effect of two types of nanoclusters on the multi-step aging behavior. The hardness of the Cu-added alloy is always higher than that of the Cu-free alloy when isothermal aging is directly performed. Furthermore, the hardness increase is due to the formation of Cluster (1) and Cluster (2) during N.A. and P.A., respectively in the both Cu-free and Cu-added alloys. Importantly, the retadation period of the hardness increase appears at the initial stage of isothermal aging at 170°C for the N.A. specimens in the both Cu-free and Cu-added alloys. It is noted that Cluster (1) does not directly transform into the β'' phase. On the other hand, the hardness directly increases in the P.A.-N.A. specimens of the both Cu-free and Cu-added alloys. It is also noted that Cluster (2) directly transforms into the β'' phase. On the other hand, there is big difference in the over-aging behavior between the Cu-free and Cu-added alloys. The Cu-added alloy shows higher thermal stability than the Cu-free alloy. It is deduced that the thermally more stable phase is formed in the Cu-added alloy than in the Cu-free alloy during over-aging condition.

Figure 6 shows the BH response with the different heat-treatment conditions in the both Cu-free and Cu-added alloys. The A.Q. specimens show higher BH response than any other specimens. There is no hardness increase during isothermal aging at 170°C for 1.2 ks if the natural aging is previously performed for 604.8 ks as called the *negative effect of two-step aging*. However, the formation of Cluster (1) is significantly suppressed due to the formation of Cluster (2) formed by the P.A. treatment at 100°C and this phenomenon causes increasement of the BH response even though the N.A. after P.A. aging is performed. It is noted that the competitively formed nanoclusters fairly affect the BH response in the both Cu-free and Cu-added alloys. In order to confirm whether Cu incorporates into the strengthening Q′ phase or not, TEM observation was performed at the under-aged condition for the N.A. specimen in the Cu-added alloy.

Figures 7(a) and (b) show the TEM and HRTEM micrographs for the Cu-added alloy aged at 170°C for 14.4 ks, respectively. Figure 7(c) shows the SADP of (a). Figure 7(d) shows the calculated diffraction pattern reported by Miao and Laughilin[14] and Chakrabarti *el al.*[11,17] The SADP in Fig. 7(c) corresponded well with the proposed calculated diffraction pattern. Namely, the Q′ phase is formed extremely earlier than the peak hardness in the Cu-added alloy.

Figure 8 shows the changes of the electrical resistivity during isothermal aging at 170°C in the both Cu-free and Cu-added alloys. Some more details of the age-hardening behaviors are confirmed due to the advantages of the experiment for the electrical resistivity such as the possible measurement of the initial stage of aging without interruption

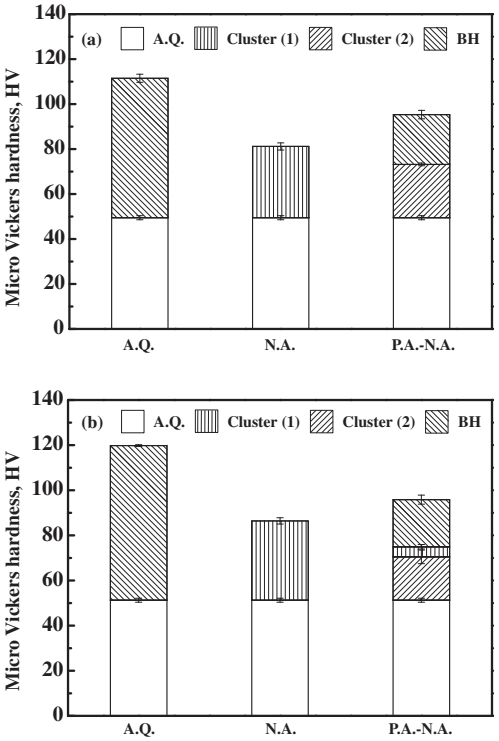

Fig. 6 Hardness changes with different heat treatment conditions in the both (a) Cu-free and (b) Cu-added alloys. BH represents aging at 170°C for 1.2 ks.

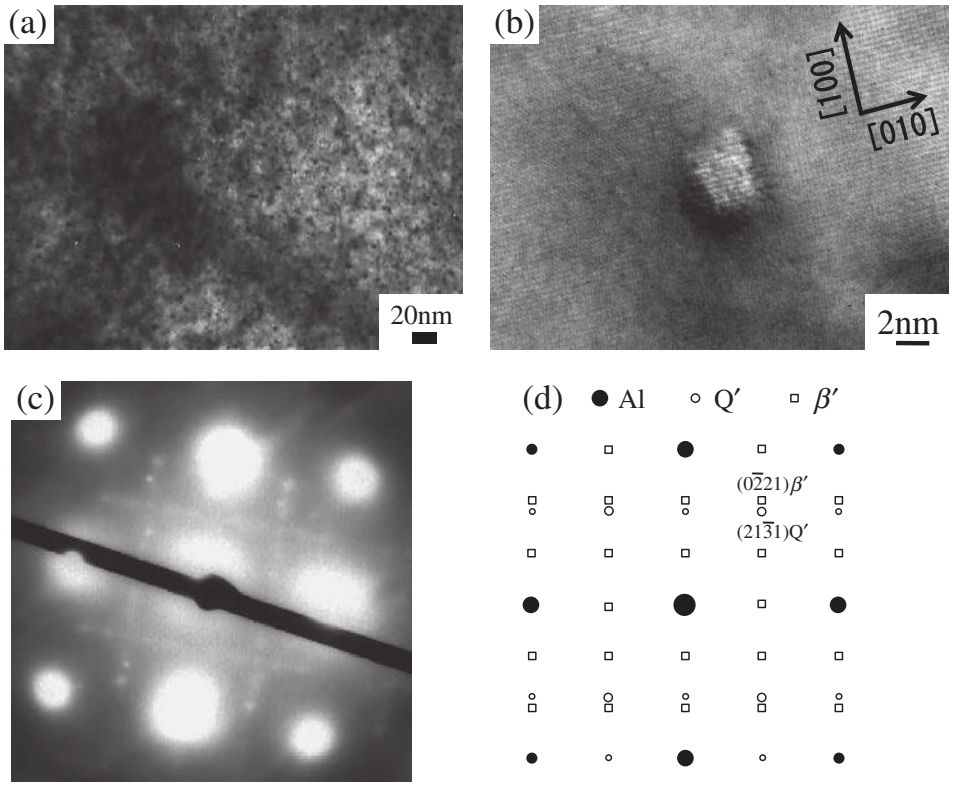

Fig. 7 (a) TEM micrograph aged at 170°C for 14.4 ks after natural aging for 604.8 ks in the Cu-added alloy, (b) HRTEM micrograph (c) SADP of (a) and (d) a calculated diffraction pattern of β' and Q′ in the Al matrix with the orientation relationships of $[100]_{Al}$ // $[0001]_{\beta'}$, $(020)_{Al}$ // $(0220)_{\beta'}$ and $[100]_{Al}$ // $[0001]_{Q'}$, $(020)_{Al}$ // $(2130)_{Q'}$.[17]

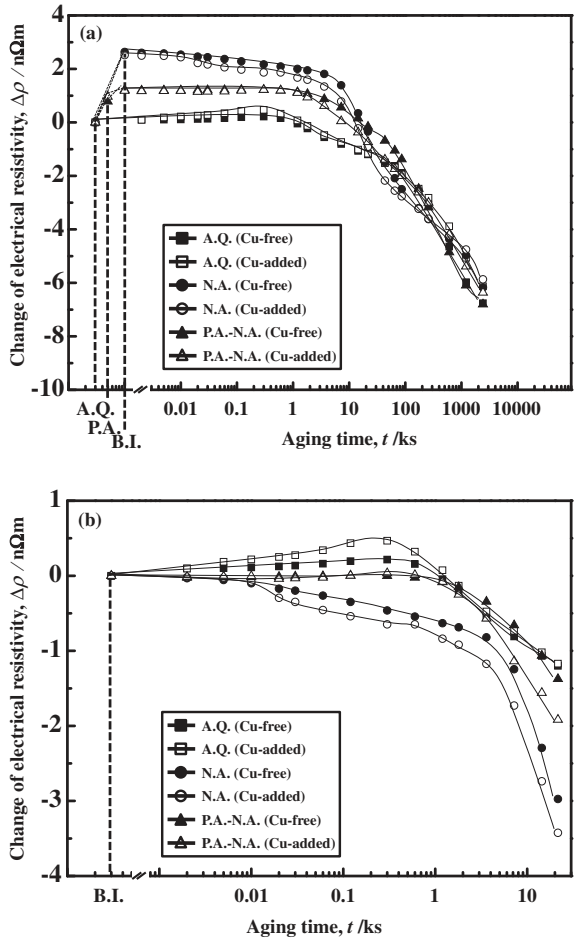

Fig. 8 Changes of electrical resistivity aged at 170°C with different heat treatment conditions in the Cu-free and Cu-added alloys: (a) changes from A.Q. and (b) early stage changes from A.Q. at 170°C. A.Q.: as-quenched, P.A.: as-pre-aged, B.I.: before isothermal aging

of the natural aging during the preperation of the specimens. Figure 8 shows that the electrical resistivity is increased due to the formation of nanoclusters during N.A. and P.A.-N.A. in the both Cu-free and Cu-added alloys. In order to understand the complicated behavior of nanoclusters before isothermal aging at 170°C with the multi-step heat treatment, electrical resistivity is normalised by the electrical resistivity before isothermal aging (B.I.) regardless of the prior heat-treatment histories in Fig. 8(b). The Cu-added alloy shows the higher increase of the electrical resistivity than the Cu-free alloy for the as-quenched condition at the initial stage of the isothermal aging at 170°C. It is noted that the Cu-added alloy produces higher number density precipitates than the Cu-free alloy at the early stage of aging at 170°C. The reason why this phenomenon occurs will be discussed in the next section. On the other hand, the elctrical resistivity for the N.A. specimens is slightly decreased in the both Cu-free and Cu-added alloys. It is plausible that thermally unstable nanoclusters are dissolved. Some more details are also discussed in the next section regarding this phenomenon. On the other hand, P.A. specimens keep a constant value of the electrical resistivity in the both Cu-free and Cu-added alloys at the early stage of aging at 170°C. As introduced in the analysis method for the electrical resistivity, the substantial decrease of the electrical resistivity is caused by the decrease of number density with increase of the volume fraction of the precipitates. The decrease of the electrical resistivity is in order of A.Q., P.A.-N.A. and N.A. specimens.

Figure 9 shows TEM micrographs aged at 170°C for 64.8 ks with the different heat-treatment conditions in the both Cu-free and Cu-added alloys. The Cu-added alloy shows the higher number density of the β'' phase than the Cu-free alloy as expected from the hardness and electrical resistivity measurements. Furthermore, P.A. specimens exhibit the higher number density of the β'' phase than the N.A. specimens due to the different transition behavior of the different types of nanoclusters. On the other hand, P.A. specimens show the lower number density of the β'' phase than the A.Q. specimens since the amount of vacancy is decreased during P.A.-N.A. in the both Cu-free and Cu-added alloys. Those microstructure changes by the different heat-treatment conditions well correspond to the results of hardness and electrical resistivity measurements.

5. Discussion

5.1 Transition behavior

It is possible to understand whether transformation from nanocluster or solute atoms into the β'' phase occurs from the DSC results. From the P.A. DSC results in the both Cu-free and Cu-added alloys, there are broadened peaks ranging from 200 to 250°C. It is deduced that there are several metatable phases with the variation of the size and chemical compositions. Namely, various kinds of metastable phases could appear with the slightly different heat-treatment procedure and alloy composition. Ravi and Wolverton[18] well summarized some information regarding the metastable phases from the viewpoint of the structure and the ratio of Mg/Si. It is noted that the transformation from Cluster (2) to the β'' phase requires lower activation energy than the A.Q. specimens from the appearence of the shoulder of the P.A. specimens. It is deduced that energetically favorable Cluster (2) possibly transforms directly into the pre-β'' phase or the β'' phase. This is the reason why the hardness during isothermal aging at 170°C after P.A.-N.A. is directly increased as confirmed in Fig. 5. On the other hand, the N.A. specimens show a retardation period as confirmed in Fig. 5. From DSC and hardness measurements, it is deduced that the structure of Cluster (2) is similar to that of the β'' phase, while the structure of Cluster (1) is different from the β'' phase. Similar phenomena are confirmed by the 3DAP analysis.[3]

Figure 10 shows the schematic diagram showing the Gibbs energy, G_t, as a funtion of aging time for the different phases. The simbols G_o, G_1, G_2, G_3, G_4, G_5 and G^* represent the Gibbs energy for the state of SSSS, Cluster (2), pre-β'', β'', β', β phases and Cluster (1), respectively. It is reasonable that more stable phase from the thermodynamic viewpoint is formed as proceeding aging even though there still exist metastable phases. Therefore, the Gibbs energy of Cluster (1) is possibly positioned between SSSS and Cluster (2) since the formation temperature of Cluster (1) is much lower than that of Cluster (2). The formation temperature of the β'' peak for the N.A. specimen is expected to be lower than for the as-quenched specimen in the both Cu-free and Cu-added

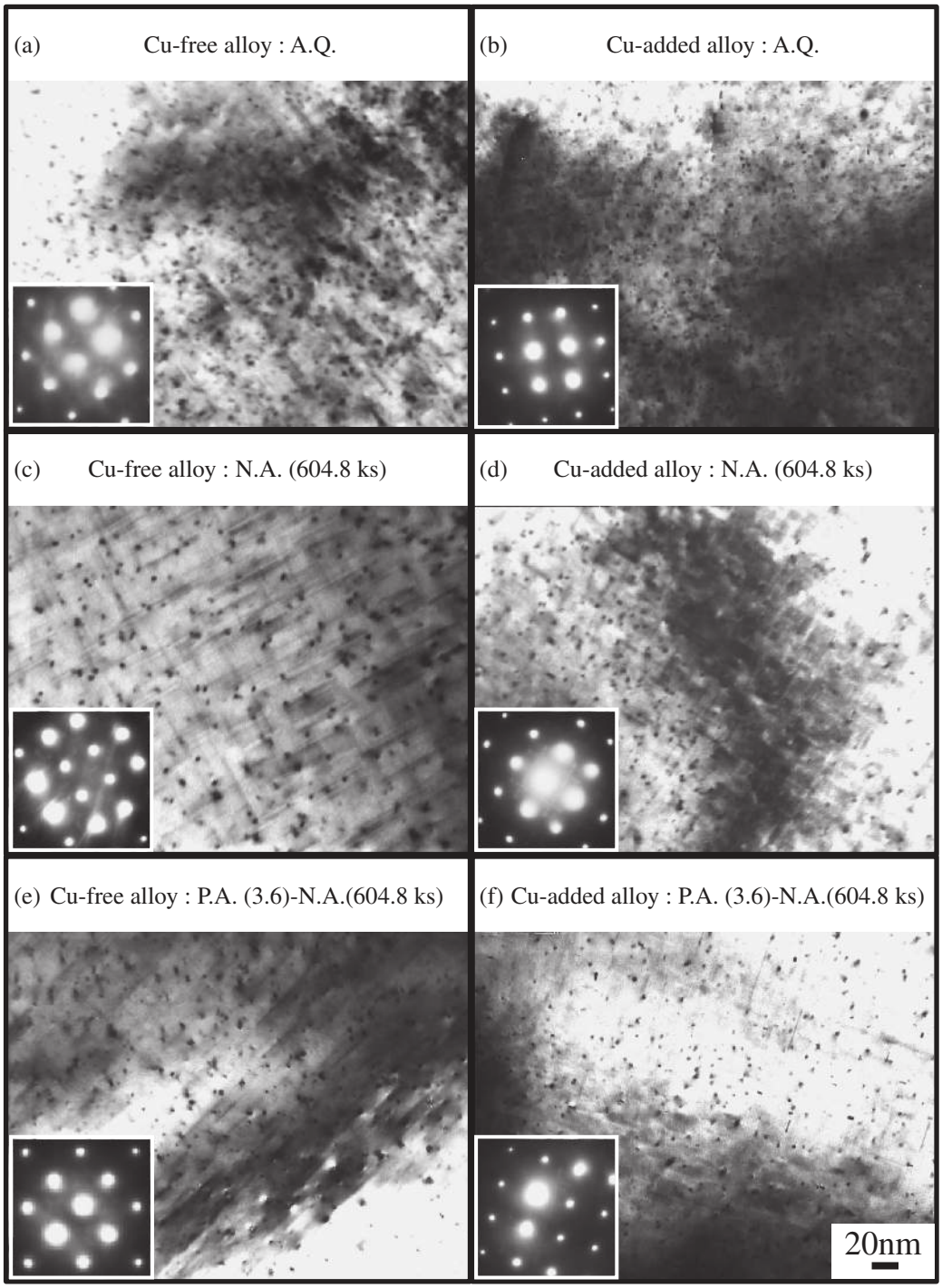

Fig. 9 TEM micrographs aged at 170°C for 64.8 ks with different heat treatment conditions in the Cu-free and (a) A.Q., (c) N.A. and (e) P.A.-N.A. and Cu-added alloy (b) A.Q., (d) N.A. (f) P.A.N.A.

alloys from the DSC results if Cluster (1) directly transforms into the β'' phase. However, the peak of the β'' phase for the N.A. is located at higher temperature as compared with the as-quenched specimen. It clearly represents that Cluster (1) cannot directly transform into the β'' phase. It is also noted that Cluster (2) can directly transform into the β'' phase from the DSC and hardness measurements.

5.2 Thermal stability of nanocluster

Different thermal stability of nanoclusters is confirmed through the electrical resistivity measurements in Fig. 8 during aging at 170°C in the both Cu-free and Cu-added alloys. A slight decrease in the electrical resistivity for the N.A. specimen is confirmed at the early stage of isothermal aging at 170°C. On the other hand, there is no decrease in the electrical resistivity for the P.A. specimen at the early stage of isothermal aging at 170°C. It is noted that small clusters or co-clusters among Si, Mg atoms and vacancies formed during N.A. is unstable during aging at 170°C. In order to understand the thermal stability of nanoclusters, critical radius, r^*, of nanoclusters is assumed. The nanoclusters smaller than r^* are easily dissolved, while those larger than

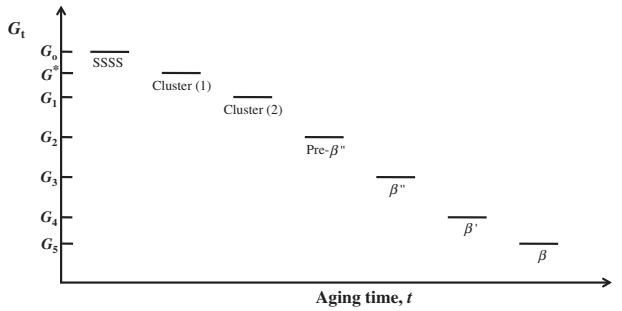

Fig. 10 Schematic diagram showing the Gibbs energy G_t of the alloy as a function of aging time.

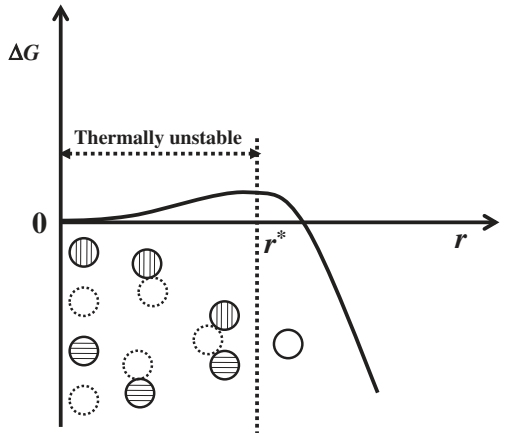

Fig. 11 Schematic diagram of the size effect of nanoclusters: ◌, ◍, ◍, ○ and r^* represent vacancy, Mg atom, Si atom, Cluster (1) and critical nucleus size, respectively.

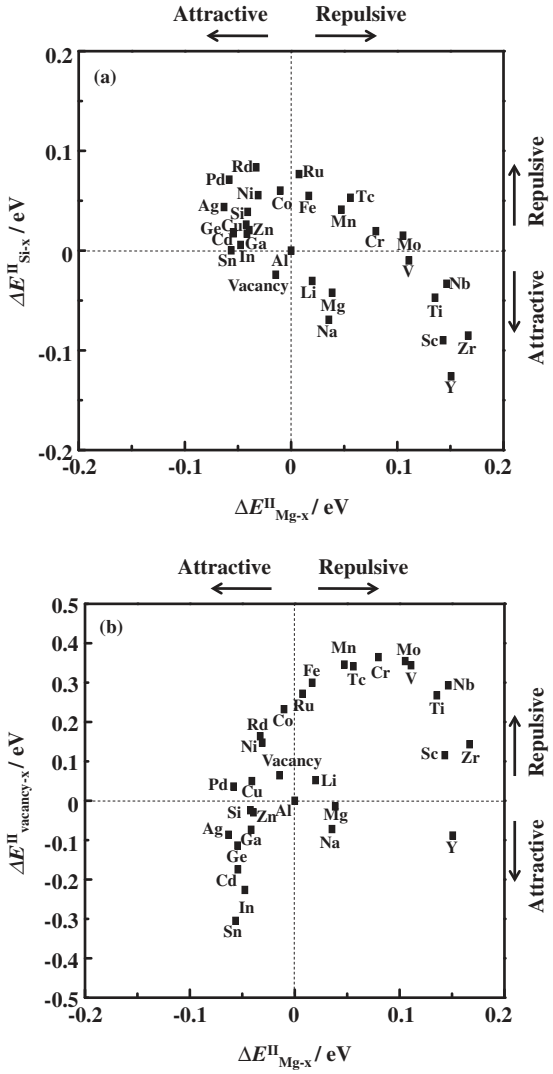

Fig. 12 Relationship between the nearest neighbor two-body interactions in Al derived from a first-principle calculation based on FPKKR-Green function method. (a) $\Delta E^{II}_{Si\text{-}x}$ and $\Delta E^{II}_{vacancy\text{-}x}$ and (b) $\Delta E^{II}_{Mg\text{-}x}$ and $\Delta E^{II}_{vacancy\text{-}x}$. See the text in detail.[6,7]

r^* remain stable. Based on the above assumption, the size of Cluster (1) which is stable at the bake-hardening condition[3] is regarded as a critical radius. Figure 11 shows the schematic diagram regarding the size effect of nanoclusters. Cluster (1) with the larger size than the critical radius contributes to hardening during the natural aging treatment and also causes the negative effect of two-step aging. It is, however, still required to investigate the nucleation and growth behavior of nanoclusters during natural aging based on the atomic scale.

5.3 Early stage of age-hardening behavior and interaction energy map

Interaction energy maps provide valuable information to estimate atomistic bonding at the initial stage of the phase decomposition in the age-hardenable Al-Mg-Si alloys. Furthermore, considered atomistic behavior is experimentally confirmed by the 3DAP analysis.[7,8] From this viewpoint, the role and effect of the Cu addition to Al-Mg-Si alloys is well interpreted. Figure 12 shows the relationship among $\Delta E^{II}_{Mg\text{-}x}$, $\Delta E^{II}_{Si\text{-}x}$, $\Delta E^{II}_{Cu\text{-}x}$ and $\Delta E^{II}_{vacancy\text{-}x}$ derived from the first-principle calculation based on the full-potential Korringa-Kohn-Rostoker (FPKKR) -Green function method. $\Delta E^{II}_{Mg\text{-}x}$, $\Delta E^{II}_{Si\text{-}x}$, $\Delta E^{II}_{Cu\text{-}x}$ and $\Delta E^{II}_{vacancy\text{-}x}$ are the nearest neighbor two-body interactions in Al between Mg and X atoms, between Si and X atoms, between vacancies and X atoms, respectively. X is labeled beside a plot, corresponding to a microalloying element in Al-Mg-Si-X alloys.[6,7] In the previous study, it was revealed that the formation of Cluster (1) is suppressed by the Cu addition at the early stage of natural aging in an Al-Mg-Si alloy.[10] Cu suppresses the formation of Cluster (1) since Cu has repulsive with Si and vacancy calculated by the two-body interaction energy described in Fig. 12 in terms of that Cluster (1) consists of Si-vacancy rich clusters.[19] However, Cu possibly incorporates into Cluster (1) since Cu has strongly attractive with Mg in the middle and later stages of N.A. Therefore, the Cu-added alloy enhances the growth of Cluster (1) as confirmed by the hardness and DSC measurements.[10] On the other hand, Cu enhances the formation of Cluster (2) since Cu has strongly attractive with Mg calculated by the two-body interaction energy described in Fig. 12 in terms of that Cluster (2) consists of Mg-Si-vacancy co-clusters.[19] Therefore, the first-principle calculation provides quite useful information to estimate the two-body interaction energies among solute atoms and vacancies. The two-body interaction energies contribute to the under-

standing of the nanocluster formation behavior at the early stage of the phase decomposition in the age-hardenable Al-Mg-Si alloys.

6. Conclusions

Effects of the Cu addition on the behavior of nanoclusters during multi-step aging in Al-Mg-Si alloys is discussed based on the experimentally obtained age-hardening phenomena.

(1) Cu increases the number density of the β'' phase and refine the precipitate microstructure. Besides, the Cu-added alloy represents higher thermal stability during over-aging than the Cu-free alloy.
(2) The formation of Cluster (1) is significantly suppressed by the formation of Cluster (2) through the pre-aging treatment at 100°C in the both Cu-free and Cu-added alloys.

Acknowledgement

The present authors are grateful to Furukawa-Sky Aluminum Corporation for material supply and Dr. Shinji Muraishi of Tokyo Institute of Technology for his help of TEM operation.

REFERENCES

1) G. B. Burger, A. K. Gupta, P. W. Jeffrey and D. J. Lloyd: Mater. Charact. **35** (1995) 23–39.
2) G. A. Edwards, K. Stiller, G. L. Dunlop and M. J. Couper: Acta Mater. **46** (1998) 3893–3904.
3) A. Serizawa, S. Hirosawa and T. Sato: Mater. Sci. Forum **519–521** (2006) 245–250.
4) A. Serizawa, S. Hirosawa and T. Sato: Metall. Mater. Trans. A **39A** (2008) 243–251.
5) T. Sato, S. Hirosawa, K. Hirose and T. Maeguchi: Metall. Mater. Trans. A **31A** (2003) 2745–2755.
6) T. Hoshino and F. Nakamura: J. Metastab. Nanocrystal. Mater. **24–25** (2005) 237–240.
7) S. Hirosawa, F. Nakamura, T. Sato and T. Hoshino: JILM **56** (2006) 621–628.
8) S. Hirosawa, F. Nakamura and T. Sato: Mater. Sci. Forum **519–521** (2006) 215–520.
9) S. Hirosawa, F. Nakamura and T. Sato: Mater. Sci. Forum **561–565** (2007) 283–286.
10) J. H. Kim and T. Sato: J. Nanosci. Nanotechnol. **11** (2011) 1319–1322.
11) D. J. Chakrabarti and D. E. Laughlin: Prog. Mater. Sci. **49** (2004) 389–410.
12) J. Man, L. Jing and S. G. Jie: J. Alloy. Compd. **437** (2007) 146–150.
13) K. Matsuda, Y. Uetani, T. Sato and S. Ikeno: Metall. Mater. Trans. A **47** (2001) 833–837.
14) M. F. Miao and D. E. Laughlin: Metall. Mater. Trans A **31A** (2000) 361–371.
15) K. Osamura, Y. Hiraoka and Y. Murakami: Philos. Mag. **28** (1973) 809–825.
16) M. F. Miao and D. E. Laughlin: Scr. Mater. **40** (1999) 873–878.
17) D. J. Chakrabarti, B. K. Cheong and D. E. Laughlin: Automotive Alloys II, Proc. TMS Annual Meeting, San Antonio, TX, ed. Subodh K. Das, (TMS, Warrendale, 1998) pp. 27–44.
18) C. Ravi and C. Wolverton: Acta Mater. **52** (2004) 4213–4227.
19) K. Yamada, T. Sato and A. Kamio: Mater. Sci. Forum **331–337** (2000) 669–674.